

7th Groundwater Symposium of the  
International Association for Hydro-Environment Engineering and Research (IAHR)

## Porous gravity currents of non-Newtonian fluids within confining boundaries

V. Ciriello<sup>a</sup>, S. Longo<sup>b</sup>, L. Chiapponi<sup>b</sup> and V. Di Federico<sup>a\*</sup>

<sup>a</sup>DICAM-Università di Bologna, Viale Risorgimento 2, 40136 Bologna, Italy

<sup>b</sup>DICATeA-Università di Parma, Parco Area delle Scienze 181/A, 43124 Parma, Italy

### Abstract

Motion of non-Newtonian gravity currents in horizontal impermeable channels filled with a porous material is investigated theoretically and experimentally. A constant or time-variable volume of fluid, characterized rheologically by the Ostwald-de Waele constitutive equation, is released from a point source into a channel of uniform cross-section, whose boundary height is described by a monomial relationship. The mathematical problem is formulated and solved at the Darcy scale coupling the local mass balance equation with a modified Darcy's law, taking into account the nonlinearity of the rheological equation. The resulting non-linear ODE is integrated numerically in the general case; for the release of a constant volume, a closed-form analytical solution is derived. Earlier results for Newtonian currents inside confining boundaries and power-law currents in two-dimensional geometry are generalized. The experiments were conducted in a transparent channel of semi-circular cross-section filled with uniform size glass ballotini. The position of the current front, recorded by a photo camera, was generally in a good agreement with the theory. The propagation of the current is described by  $L \sim t^{F_2}$  where  $F_2$  is a scalar depending on (i) the time exponent of the volume of fluid in the current,  $\alpha$ , (ii) the geometry of the channel, parameterized by  $\beta$  and (iii) the exponent  $n$  of the rheological equation. It is found that for a critical value  $\alpha_c = n/(n+1)$ ,  $F_2$  is independent on the shape of the channel; for  $\alpha < \alpha_c$ ,  $F_2$  is a decreasing function of  $\beta$ ; the reverse is true for  $\alpha > \alpha_c$ . Upon comparing results with free-surface viscous flow in open channels, it is found that: (i) the same expression for  $\alpha_c$  holds; (ii) the exponent  $F_2$  increases or decreases monotonically with  $\beta$ , while for the triangular section ( $\beta = 1$ ) in open channels, a maximum or minimum value of  $F_2$  is attained for  $\alpha < \alpha_c$  and  $\alpha > \alpha_c$ , respectively.

© 2015 The Authors. Published by Elsevier B.V. This is an open access article under the CC BY-NC-ND license (<http://creativecommons.org/licenses/by-nc-nd/4.0/>).

Peer-review under responsibility of the Scientific Committee of the IAHR Groundwater Symposium 2014

**Keywords:** Non-Newtonian; power-law; porous media; gravity current; self-similar solution; channel; experiments

\* Corresponding author. Tel.: +39-051-2093750; fax: +39-051-6448346.

E-mail address: [vittorio.difederico@unibo.it](mailto:vittorio.difederico@unibo.it).

## 1. Introduction

Porous gravity currents, determined by a fluid intruding into a porous formation initially saturated with a fluid of different density, are widely studied since they occur in many environmental processes such as enhanced oil and heat recovery, groundwater remediation, carbon dioxide sequestration, and saltwater intrusion (see [1] and references therein). The literature is rich in analytical, numerical and experimental approaches to gravity-driven flows in porous media generated by the release of a time-variable volume of fluid. The flow is often described under the thin current assumption, neglecting the dynamics of the ambient fluid, and considering simple geometries and propagation over an impermeable bottom [2-4]. The mathematical problem is solved by means of self-similar solutions, describing the intermediate asymptotic behaviour of the current when the solution is no longer dependent on the specific initial and/or boundary conditions. Comparison of theory with experiments usually provides good results for the front end speed and current profile, except at the beginning of the process and near the injection zone. A step forward consists in including the effect of confining boundaries to represent flow in porous channels [5], whose shape is shown to affect significantly the propagation rate.

Another important progress in the study of porous gravity currents consists in considering non-Newtonian behaviour, to represent the rheology of, e.g., polymeric suspensions in enhanced oil recovery; pollutants in environmental modelling; muds in well drilling; crude oil in reservoir engineering; fluid carriers for nanoparticles in soil remediation. Solutions for non-Newtonian gravity currents of power-law fluids are derived in planar and radial geometry by [6-7], and experimentally confirmed by [8].

Akin to Newtonian applications, the channel geometry is expected to impact the propagation of gravity currents of non-Newtonian fluids in porous media. To explore the combined effect of rheology and channel geometry, we consider an Ostwald-de Waele constitutive equation for the fluid, and a channel of uniform cross-section, whose boundary height is described by a monomial relationship. The mathematical problem is formulated in Section 2; a self-similar solution is derived in Section 3 and discussed in Section 4. To verify the theoretical results, a set of experiments is designed and carried out in a circular horizontal channel under constant volume flux conditions; comparison with theory is described in Section 5. Section 6 provides some concluding remarks.

## 2. Problem formulation

We study the gravity-driven flow of a viscous non-Newtonian fluid of power-law behaviour, described in simple shear flow by  $\tau = \tilde{\mu}\dot{\gamma}^n$ , being  $\tau$  and  $\dot{\gamma}$  the shear stress and shear rate,  $n$  the behaviour index and  $\tilde{\mu}$  the consistency index;  $n < 1$  and  $n > 1$  describe shear-thinning and shear-thickening fluids, respectively, while for  $n = 1$  Newtonian rheology is recovered and  $\tilde{\mu}$  reduces to dynamic viscosity  $\mu$ . The power-law model usually provides an accurate approximation in an intermediate range of shear rates (e.g.  $0.1\text{-}5\text{ s}^{-1}$ , as demonstrated in [9]). The intruding fluid, of density  $\rho + \Delta\rho$ , is released at the origin of a horizontal rectilinear channel of fixed cross-section, filled with a homogeneous porous medium saturated with a second fluid of lesser density  $\rho$ . The height of the gravity current is considered to be a small fraction of its length and of the saturated layer height, the hydrostatic assumption is assumed to hold, and mixing and surface tension effects are neglected. The channel geometry is shown in Figure 1a. The channel wall (Figure 1b) is given by the generic power-law relationship  $b(y) = h_c a (y/a)^\beta$ , where  $\beta$  is a shape parameter,  $a$  is a length scale, and  $h_c$  is a dimensionless constant. In such a channel, the height  $h(x, t)$  and half width  $W(x, t)$  of the current are related as  $h/a = h_c (W/a)^\beta$ , implying  $W(x, t) = (h/h_c)^{1/\beta} a^{(\beta-1)/\beta}$ ;  $\beta = 1$  corresponds to a triangle, while  $\beta \rightarrow \infty$  represents a rectangle of half width  $a$ , recovering two-dimensional flow along a flat surface [2] as a special case.

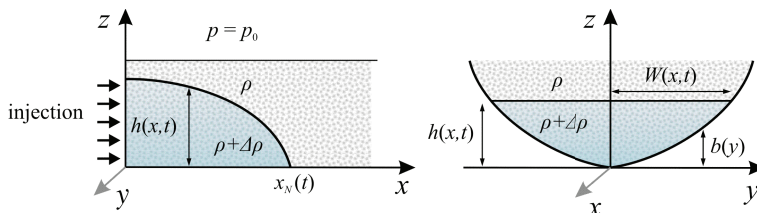


Fig. 1. (a) Coordinate system; (b) Channel cross-section, y-z plane

Under these hypotheses, the local mass balance equation is given by [5]

$$\phi \frac{\partial}{\partial t} (A_c h^{(\beta+1)/\beta}) + \frac{\partial}{\partial x} (u_x A_c h^{(\beta+1)/\beta}) = 0; A_c = \frac{2\beta}{\beta+1} \frac{a^{(\beta-1)/\beta}}{h_c^{1/\beta}}, \tag{1a,b}$$

where  $\phi$  is the medium porosity and  $u_x$  the Darcy velocity in the x direction, given by [10]

$$u_x(x,t) = (\Lambda \Delta \rho g)^{1/n} k^{(1+n)/(2n)} \left(-\frac{\partial h}{\partial x}\right)^{1/n}; \Lambda = \Lambda(\phi, \tilde{\mu}, n) = \frac{8^{(n+1)/2}}{2} \left(\frac{n}{3n+1}\right)^n \frac{\phi^{(n-1)/2}}{\tilde{\mu}}, \tag{2a,b}$$

in which the hydrostatic assumption was employed. Substituting (2a) in (1a) yields

$$v^* \frac{\partial}{\partial x} \left[ h^{F_1} \left(-\frac{\partial h}{\partial x}\right)^{1/n} \right] = -\frac{\partial (h^{F_1})}{\partial t}; F_1 = \frac{\beta+1}{\beta}; v^* = \frac{(\Lambda \Delta \rho g)^{1/n} k^{(1+n)/2n}}{\phi}, \tag{3a,b,c}$$

where  $v^*$  is the velocity scale, and the factor  $F_1$  encapsulates the cross-section shape; for flow in very wide rectangular channels,  $F_1 \rightarrow 1$  [2]. The current volume at any time  $t$  is given by  $Qt^\alpha$ , with  $Q$  and  $\alpha$  being constant;  $\alpha = 0$  implies the instantaneous release of a fixed volume and  $\alpha = 1$  a constant volume flux. The global continuity equation and the condition at the edge  $x_N(t)$  of the current read, respectively

$$\phi \int_0^{x_N(t)} A_c h^{F_1} dx = Qt^\alpha; h(x_N(t), t) = 0. \tag{4a,b}$$

Upon introducing the dimensionless variables  $t' = t/t^*$ ;  $x' = x/x^*$ ;  $x'_N = x_N/x^*$ ;  $h' = h/x^{*\beta}$ , where the time and space scales are defined via the velocity scale respectively as  $t^* = (Q/(\phi v^{*3}))^{1/(3-\alpha)}$ ;  $x^* = v^* t^*$ ,

equations (3a), (4a) and (4b) become respectively

$$\frac{\partial}{\partial x'} \left[ h'^{F_1} \left( -\frac{\partial h'}{\partial x'} \right)^{1/n} \right] = -\frac{\partial (h'^{F_1})}{\partial t'}; \int_0^{x'_N(t')} A'_c h'^{F_1} dx' = t'^{\alpha}; A'_c = \frac{2\beta}{\beta+1} \frac{1}{h_c^{1/\beta}} \left( \frac{a}{x^*} \right)^{\beta}; h'(x'_N(t'), t') = 0. \quad (5a,b,c,d)$$

In the sequel, primes are removed for the sake of brevity. For  $\alpha = 3$ , the time scale is no longer valid and  $(Q/\phi)^{1/3}$  emerges as an additional velocity scale; a new set of dimensionless variables needs to be defined along the lines of [11]; refer to [7] for this case.

### 3. Self-similar solution

To find a similarity solution, we note that (5a)-(5b) provide for the length and height of the current  $L$  and  $H$  the scalings  $L \sim T^{(\alpha+nF_1)/[F_1(n+1)+1]} / A_c^{1/[F_1(n+1)+1]}$ ,  $H \sim T^{[\alpha(n+1)-n]/[F_1(n+1)+1]} / A_c^{(n+1)/[F_1(n+1)+1]}$ . This suggests the introduction of the similarity variable and scaling for the current height as

$$\eta = A_c^{F_4} x/t^{F_2}; h(x,t) = A_c^{-(n+1)F_4} \eta_N^{F_5} t^{F_3} \Psi(\xi), \quad (6a,b)$$

where  $\eta_N$  is the value of the similarity variable at the current edge,  $\xi = \eta/\eta_N$  the reduced similarity variable,  $\Psi(\xi)$  the shape function, and the factors  $F_i$  ( $i = 2-5$ ) are given by

$$F_2 = \frac{\alpha\beta + (\beta+1)n}{(\beta+1)(n+1) + \beta}; F_3 = \frac{\beta[\alpha(n+1) - n]}{(\beta+1)(n+1) + \beta}; F_4 = \frac{\beta}{(\beta+1)(n+1) + \beta}; F_5 = n+1. \quad (7a,b,c,d)$$

Substituting (6a,b) in (5a,b,d) yields respectively

$$\frac{d}{d\xi} \left[ \Psi^{F_1} \left( -\frac{d\Psi}{d\xi} \right)^{1/n} \right] - F_1 \Psi^{F_1-1} \left( F_2 \frac{d\Psi}{d\xi} - F_3 \Psi \right) = 0; \eta_N = \left( \int_0^1 \Psi^{F_1} d\xi \right)^{-F_4}; \Psi(1) = 0. \quad (8a,b,c)$$

Once  $\eta_N$  is determined, the extension of the gravity current is given by  $x_N(t) = (\eta_N/A_c^{F_4}) t^{F_2}$ . For a current of constant volume ( $\alpha = 0$ ), equations (8a,b,c) can be solved analytically yielding

$$\Psi(\xi) = \frac{F_{20}^n}{n+1} (1 - \xi^{F_5}); \eta_N = \left[ \frac{F_5^{F_1}}{F_1 F_4 F_{20}^{nF_1}} \frac{\Gamma(1/(F_4 F_5))}{\Gamma(1/F_5) \Gamma(F_1)} \right]^{F_4}; F_{20} = F_2(\alpha = 0) = \frac{(\beta+1)n}{(\beta+1)(n+1) + \beta}, \quad (9a,b,c)$$

where  $\Gamma(\cdot)$  is the gamma function. For the case  $\alpha \neq 0$ , Equations (8a,b,c) are solved numerically.

Governing equations and results include as special cases: i) the Newtonian fluid ( $n = 1$ ) [5]; ii) the infinitely wide rectangular section ( $F_1 = 1$ ,  $\beta \rightarrow \infty$ ) [6]. For  $n = 1$ ,  $F_1 = 1$ , the results of [2] are recovered.

#### 4. Discussion of results

The time exponent of the front end position,  $F_2$ , is a function of the time exponent of the fluid volume,  $\alpha$ , of the geometry of the channel, parameterized by  $\beta$ , and of the fluid behaviour index,  $n$ . Figure 2 shows this dependency for a shear-thinning fluid with  $n = 0.5$ . It is seen that for a given fluid and channel shape,  $F_2$  always increases with  $\alpha$ . For a given value of  $\alpha$ , the effect of the shape parameter  $\beta$  differs if  $\alpha$  is above or below a critical value  $\alpha_c = n/(n + 1)$ . In the former case,  $F_2$  increases with  $\beta$ ; in the latter case, the reverse is true. If  $\alpha = \alpha_c$ , the shape of the cross-section does not affect the value of  $F_2$  and it results  $F_2 = n/(n + 1)$ . The height of the current is  $\sim t^{F_2}$  and it increases or decreases with time depending whether  $\alpha > \alpha_c$  or  $\alpha < \alpha_c$ .

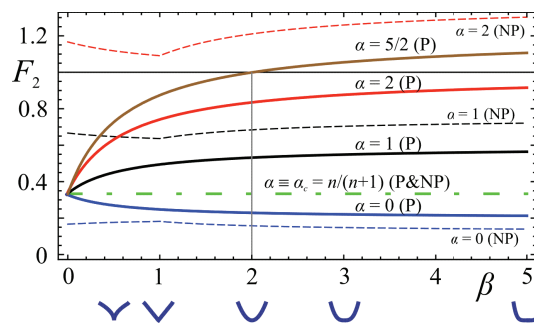


Fig. 2. Values of  $F_2$  as a function of  $\beta$  for different  $\alpha$ , for a shear-thinning fluid with  $n = 0.5$ . The solid lines (P) refer to channels filled with a porous medium, the dashed lines (NP) to open channels. The line corresponding to  $\alpha = 5/2$  indicates that the current is accelerating ( $F_2 > 1$ ) in channels with  $\beta > 2$ . Below the  $\beta$  axis, the channel shapes corresponding to different  $\beta$  are sketched.

The qualitative behaviour of the exponent  $F_2$  against  $\beta$  is the same if different values of the rheological index  $n$  are considered (not shown), except that the critical value  $\alpha_c$  increases with  $n$ , tending to 0 for very shear-thinning fluids ( $0 < n \ll 1$ ) and to 1 for very shear-thickening fluids ( $n \gg 1$ ); for Newtonian fluids ( $n = 1$ ) the results of [5] are recovered, with  $\alpha_c = 1/2$ . Figure 2 also depicts for comparison (dashed lines) the time exponent  $F_2$  obtained for laminar gravity currents of non-Newtonian power-law fluid flowing in open channels [12]. It is seen that the critical value of  $\alpha$  is common to both flows; in porous channels, the exponent  $F_2$  increases or decreases monotonically with  $\beta$ , while in open channels it attains a maximum or minimum value for the triangular section ( $\beta = 1$ ) when  $\alpha < \alpha_c$  and  $\alpha > \alpha_c$  respectively. The different behaviour is due to the main role played by the shape of the cross-section for free surface flows under the validity of Stokes equation, with an abrupt change in behaviour (at least in the analytical model) for  $\beta = 1$  (triangular section), which is absent in porous channels.

To evaluate whether the current accelerates or decelerates, the behaviour of  $F_2 - 1$  is examined. It is seen that the front end accelerates or decelerates depending whether  $\alpha$  is above or below a limit value  $\alpha_l = 2 + 1/\beta$ , which is not influenced by the rheology of the fluid. The average pressure gradient driving the motion, being proportional to the ratio between the average current height and length, varies with time as  $t^{F_3 F_2}$ , and hence increases or decreases with time for  $\alpha > \alpha_l$  or  $\alpha < \alpha_l$ . For triangular or concave cross-

sections with  $\beta \geq 1$ , the limit value  $\alpha_l$  varies between 2 for the rectangular cross-section ( $\beta \rightarrow \infty$ ) and 3 for the triangular one ( $\beta=1$ ). Hence, in the range  $2 \leq \alpha \leq 3$  the current can be accelerated or decelerated depending on the channel shape, as earlier noted by [5] and shown in Figure 2 for  $\alpha = 5/2$ ; the current is always accelerated for  $\alpha > 3$ . For convex cross-sections with  $0 < \beta < 1$ , the current is always decelerated if  $\alpha < 3$ , whereas an accelerated current can be obtained if  $\alpha > \alpha_c > 3$ . In particular for  $\alpha = \alpha_c$ , the current is always decelerated.

The overall behaviour of the current can be interpreted by considering that for  $\alpha > \alpha_c$  the current height increases with time ( $h \sim t^{F3>0}$ ): however if the volume of fluid grows at a sufficient rate (i.e.,  $V \sim t^{>4>\alpha_c}$ ) the front end of the current can be accelerated ( $x_N \sim t^{F2>1}$ ), otherwise it is decelerated. For  $\alpha < \alpha_c$ , the height of the current always decreases in time, and the volume of injected fluid will never be sufficient to accelerate the front end. In turn, acceleration or deceleration of the current is related to the average gradient pressure through the Darcy-like law (2a) and its interaction with the mass balance equation (1a)-(2a), with the rheology of the fluid involved only in the limit value of  $\alpha$ .

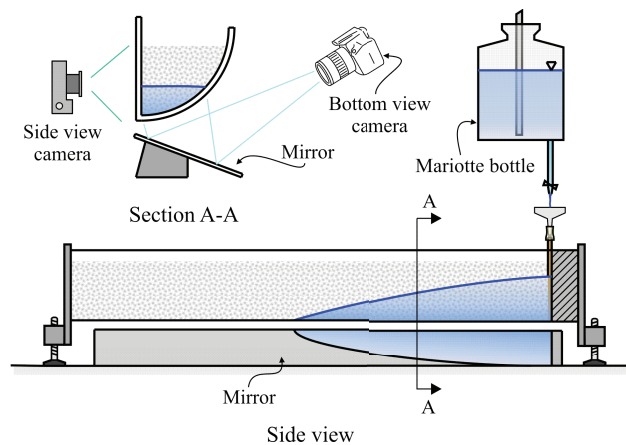


Fig. 3. Sketch of the experimental setup.

## 5. Experimental investigation

Theoretical results are validated against experiments conducted in the Hydraulics Laboratory of the University of Parma. The advancement of currents of shear-thinning fluids within a semi-circular channel, filled with a porous medium composed of glass ballotini, is measured and compared with the similarity solution for the case  $\beta = 2$ , approximating the semi-circular cross-section when the current width is small if compared to the channel radius. The ambient fluid is air. Four different diameters of the beads  $d = 1 - 4$  mm, and different fluids with behaviour index and density in the ranges  $n = 0.42 - 0.75$  and  $1080 - 1174 \text{ kg m}^{-3}$  are tested, with constant flow discharge varying from  $0.233$  to  $1.04 \text{ ml s}^{-1}$ .

The experimental apparatus (Figure 3) consist of a quarter-circle cross-section channel made of Polymethyl methacrylate, a transparent thermoplastic, with radius  $9.5 \text{ cm}$  and length  $200 \text{ cm}$ . The channel is supported with four adjustable feet to control its longitudinal and transversal inclination. The glass beads are gently poured in the channel with gravity acting as the sole compaction force. The non-Newtonian fluid is prepared mixing Glycerol, water and Xanthan gum at varying concentrations in order to obtain different rheological parameters; ink is added to enable visualization. The rheometric parameters of the fluid are measured in the low shear-rate range ( $< 5 \text{ s}^{-1}$ ) with a parallel plate rheometer; the mass density is measured by a pycnometer. The fluid is injected through a cylindrical zone positioned vertically

at one end of the channel, with the supply system represented by a Mariotte bottle and a control valve. The injected flow rate is measured at the beginning and end of the test to check its constancy, by weighing the volume of fluid exiting the bottle and collected during a given time interval. The position of the current is recorded via a high-resolution photo camera, with a time step of 10÷60 s between two consecutive shots. Another camera is used to record the profile of the current. A software allows image analysis to detect the current profile and transform pixel positions into metric coordinates. A correction is also applied to account for the effect of the capillary fringe.

Table 1. Parameter values for experiments in a horizontal channel of circular cross-section.

Exp. #	$d$ (mm)	$\rho$ (kg m <sup>-3</sup> )	$n$ (.)	$\tilde{\mu}$ (Pa s <sup><math>n</math></sup> )	$Q$ (ml s <sup>-1</sup> )	$\Delta t$ (s)	duration (s)
1	2	1160	0.42	0.36	0.734	10	430
2	2	1160	0.42	0.36	1.04	10	500
3	2	1160	0.42	0.67	0.680	30	2700
4	3	1160	0.42	0.67	0.460	60	3900
5	3	1135	0.66	0.33	0.430	60	5280
6	3	1135	0.66	0.33	0.275	60	7380
7	4	1135	0.66	0.33	0.233	60	4560
8	4	1136	0.66	0.34	0.428	60	5700
9	1	1136	0.66	0.30	0.430	60	2100
10	1	1080	0.70	0.067	0.305	60	4440
11	1	1135	0.75	0.018	0.140	60	8880
12	3	1135	0.75	0.023	0.583	60	1920

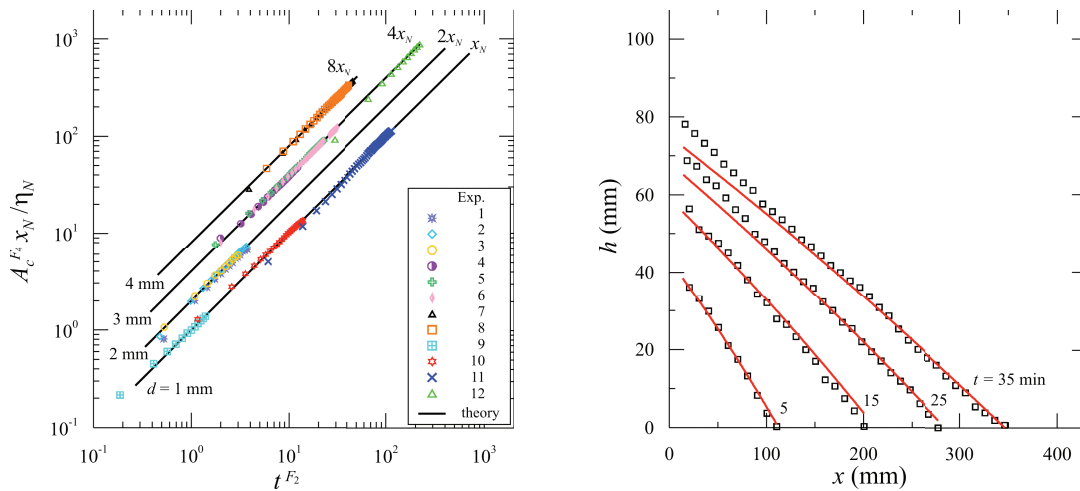


Fig. 4. Experimental results (symbols) versus theoretical results (solid curves). a) The scaled dimensionless front end position as a function of dimensionless time for all tests. The data for different diameter of the beads have been multiplied by a factor 2, 4 and 8 in order to be separated in the diagram. b) The profile of the current at different times for Experiment 10.

A series of 12 experiments is performed in a horizontal porous channel of circular cross-section. The position over time of the front end of the current is investigated for all experiments, while the analysis of the profile of the current was performed for a limited subset thereof. Table 1 lists the experimental parameters. The porosity  $\phi = 0.37$  is held constant across all tests, and the intrinsic permeability of the porous medium is computed with the Kozeny-Carman equation  $k = \phi^3 d^2 / ([180(1 - \phi)^2])$ . Figure 4a shows the scaled non-dimensional position of the front end  $x_N$  against time in log-log scale for all experiments.

The experimental results, indicated by symbols, collapse satisfactorily onto the theoretical lines, with some discrepancy at early times. Figure 4b shows the profiles of the current at different times for one of the experiments (#10). One experimental point out of ten is represented for a clear visualization. The agreement is generally fairly good, with the most relevant discrepancies near the origin, where the injection well is installed. Moreover, the assumptions of horizontal velocities and thin current are invalid in this zone; this local behaviour, however, does not affect the body of the current.

## 6. Conclusion

The propagation of a thin current of non-Newtonian power-law fluid in a horizontal porous channel of assigned cross-section is amenable to a novel similarity solution if the channel boundary and the volume of the current are described by power functions. The current front and profile are obtained in closed form for a current of constant volume, and numerically in the general case. Earlier results are recovered for Newtonian flow in porous channels of given geometry, or non-Newtonian porous flow in plane geometry.

The time advancement of the nose of the current for a given fluid is controlled by the critical value  $\alpha_c$  of the volume exponent  $\alpha$ . For  $\alpha > \alpha_c \equiv n/(n+1)$  the current is faster in cross-sections with a flatter bottom (increasing  $\beta$ ) whereas for  $\alpha < \alpha_c$  the current is faster in narrower channels ( $\beta \rightarrow 0$ ). The thickness of the current at a given location follows the same trend. A second limit value of  $\alpha$ ,  $\alpha_l \equiv 2 + 1/\beta$ , determines whether the current is accelerated or decelerated, regardless of fluid rheology. This second limit also discriminates between an average gradient pressure increasing or decreasing with time.

The theory is supported by experiments conducted at constant volume flux in semi-circular porous channels, with different values of permeability and volume discharge, and employing different shear-thinning fluids. The rheology of the fluid was assessed independently with a rheometer. Results for the current front and height over time agree well with the theoretical predictions, with discrepancies within the experimental error. Deviations from theory occur near the origin in space and time.

## References

- [1] Ciriello V, Di Federico V. Similarity solutions for flow of non-Newtonian fluids in porous media revisited under parameter uncertainty. *Adv Water Res* 2012;43:38-51.
- [2] Huppert HE, Woods AW. Gravity-driven flows in porous layers. *J Fluid Mech* 1995;292:55-69.
- [3] King SE, Woods AW. Dipole solutions for viscous gravity currents: theory and experiments. *J Fluid Mech* 2003;483:91-109.
- [4] Lyle S, Huppert HE, Hallworth M, Bickle M, Chadwick A. Axisymmetric gravity currents in a porous medium. *J Fluid Mech* 2005;543:293-302.
- [5] Golding MJ, Huppert HE. The effect of confining impermeable boundaries on gravity currents in a porous medium. *J Fluid Mech* 2010;649:1-17.
- [6] Di Federico V, Archetti R, Longo S. Similarity solutions for spreading of a two-dimensional non-Newtonian gravity current in a porous layer. *J Non-Newt Fluid Mech* 2012a;177-178:46-53.
- [7] Di Federico V, Archetti R, Longo S. Spreading of axisymmetric non-Newtonian power-law gravity currents in porous media. *J Non-Newt Fluid Mech* 2012b;189-190:31-39.
- [8] Longo S, Di Federico V, Chiapponi L, Archetti R. Experimental verification of power-law non-Newtonian axisymmetric porous gravity currents. *J Fluid Mech* 2013;731:R2-1-R2-12.
- [9] Longo S, Di Federico V, Archetti R, Chiapponi L, Ciriello V, Ungarish M. On the axisymmetric spreading of non-Newtonian power-law gravity currents of time-dependent volume: an experimental and theoretical investigation focused on the inference of rheological parameters. *J Non-Newton Fluid Mech* 2013;201:69-79.
- [10] Di Federico V, Longo S, Chiapponi L, Archetti R, Ciriello V. Radial gravity currents in vertically graded porous media: theory and experiments for Newtonian and power-law fluids. *Adv Water Res* 2014;70:65-76.
- [11] Vella D, Huppert HE. Gravity currents in a porous medium at an inclined plane. *J Fluid Mech* 2006;556:353-362.
- [12] Longo S, Di Federico V, Chiapponi L. Non-Newtonian power-law gravity currents propagating in confining boundaries. *Env Fluid Mech* 2014, DOI 10.1007/s10652-014-9369-9.